ChemComm

Anthracene-based azo dyes for photo-induced proton-coupled electron transfer

Journal:	*ChemComm*
Manuscript ID	CC-COM-02-2019-001206.R1
Article Type:	Communication

Journal Name

COMMUNICATION

Anthracene-based azo dyes for photo-induced proton-coupled electron transfer

Received 00th January 20xx,
Accepted 00th January 20xx

DOI: 10.1039/x0xx00000x

www.rsc.org/

Amanda N. Oldacre[a], Craig A. Pointer[a], Shea M. Martin[a], Amanda Kemmerer[b] and Elizabeth R. Young[a,*]

Herein, we report a new donor-acceptor system for photo-induced proton-coupled electron transfer (PCET) that leverages an azo linkage as the proton-sensitive component and anthracene as a photo-trigger. Electrochemistry shows a change in the reduction potential with addition of acid. However, photochemistry is invariant to the absence or presence of acid. The anthracene and phenol/4-methoxyphenyl moieties of the azo dyes are highly conjugated, likely mitigating photo-induced charge transfer, despite sufficient driving force.

Proton-coupled electron transfer (PCET) plays a critical role in small molecule activation, energy conversion reactions in proteins and enzymes, and energy storage.[1–5] Studies of PCET reactions from the ground state are helpful to understand certain factors that govern proton and electron transfer.[6,7] However, a potential advantage can be derived from initiating PCET reactions using a photon.[8–13] Indeed, photo-induced PCET can harness energy from the sun to drive reactions that benefit from lower-energy intermediates available through PCET mechanisms. It is, therefore, imperative to design model systems that can initiate PCET from the excited state. Mechanistic understanding of PCET derived from such model systems is of utmost importance in enabling a sustainable energy economy.

Azo dyes are of interest for non-linear optical components,[14] optical data storage,[15] biological-medicinal studies,[16,17] and as materials for organic solar cells.[18] The rich synthetic versatility of azo dyes makes them compelling targets for the development of model systems for excited-state PCET. The electronic properties of azo dyes depend intimately on the protonation or deprotonation of the azo/hydrazo bonds. Azo dyes, such as azobenzene, have been studied for ground-state PCET reactions using a host of electrochemical techniques. Early studies of aromatic azo compounds showed that upon electrochemical reduction of an azobenzene, a stable anion radical was formed in aprotic media that protonated upon addition of acid.[19] The protonated species was more easily reduced a second time than the unprotonated counterpart.[19] A large positive shift in reduction potential was also observed when azobenzene was substituted with a pendant carboxylic acid functionality as a result of H-bonding.[20] Based on these ground-state PCET studies, azo dyes present a compelling target for photo-induced PCET.

To access photo-induced PCET, the photo-initiator anthracene is incorporated into the molecular design. Anthracene has been widely studied as a robust photo-oxidant. Herein, we describe the design and characterization of two anthracene-based azo dye dyads as model systems for photo-induced PCET (Scheme 1).

The syntheses of 4-(anthracen-2-yldiazenyl)phenol (azo-OH) and (anthracen-2-yl)-2-(4-methoxyphenyl)diazene (azo-OMe) were from modified literature procedures (Scheme 1).[21,22] In summary, 2-aminoanthracene was suspended in an aqueous acidic solution with sodium nitrite to generate the diazonium salt. Phenol was added under basic conditions to produce the final product, azo-OH, which was precipitated out under acidic conditions. Methylation of azo-OH was performed with iodomethane to produce azo-OMe. The structures were confirmed with ^{1}H NMR and ESI-MS (Figure S1-S4). The azo-OH and azo-OMe dyads were investigated as model systems for PCET using trifluoroacetic acid (TFA, pK_a(ACN) =8.6) as the proton source.[23]

Figure 1 shows the steady-state absorption and emission spectra of azo-OH and azo-OMe. The azo dyes show similar absorption to the parent anthracene (Figure S5), with the addition of a red-shifted broad shoulder at ≈400-500 nm due to delocalization that occurs across both the donor and acceptor moieties. Azo-OH and azo-OMe are weakly emissive with emission maxima at 477 and 476 nm, respectively.

Emission quantum yield (QY) measurements were performed on azo-OH and azo-OMe with 0 and 1 equivalents (eq) TFA in acetonitrile using anthracene in ethanol as a

[a] Department of Chemistry, Lehigh University, Bethlehem, Pennsylvania 18015, USA. Email: ery317@lehigh.edu; Fax: +1-610-758-6536.
[b] Department of Chemical and Physical Sciences, Cedar Crest College, Allentown, PA 18104.
Electronic Supplementary Information (ESI) available: experimental details. See DOI: 10.1039/x0xx00000x

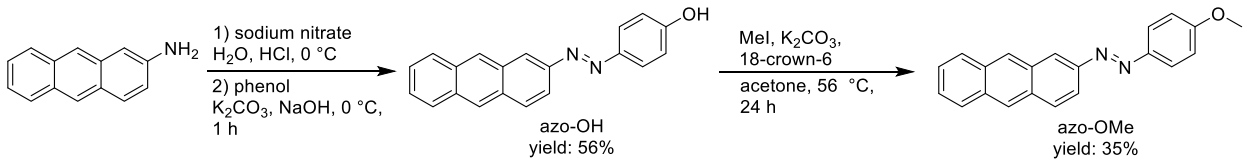

Scheme 1. Synthesis of azo-OH and azo-OMe.

standard (QY = 28%) (Table 1). Measurements were performed using samples with absorption at or below 0.1 AU to reduce reabsorption from the sample. Both azo dye dyads showed low QY. The QY of azo-OH and azo-OMe are 0.55% and 0.33%, respectively. Additions of TFA to each sample showed very little influence on the QY. The QY of azo-OH and azo-OMe with 1 eq TFA increased to 0.79% and 0.37%, respectively. The emission QY in 1 eq TFA sample is essentially the same as the 0 eq TFA sample within experimental error.

The redox properties of azo-OH and azo-OMe were investigated in acetonitrile with cyclic voltammetry (CV) and differential pulse voltammetry (DPV). Cyclic voltammograms of both azo dyes with 0 (*solid*) and 1 (*dashed*) equivalents (eq) of TFA are shown in Figure 2. Under aprotic and inert conditions, two irreversible oxidation events at ≈1.0 and 1.5 V vs $Fc^{+/0}$ and two irreversible reduction events at ≈−1.2 and −1.8 V vs $Fc^{+/0}$ are observed for azo-OH. Upon the addition of TFA, an irreversible reduction event is observed at −0.8 V vs $Fc^{+/0}$, a 400 mV shift positive. In the absence of TFA, two irreversible oxidation events at ≈1.0 and 1.3 V vs $Fc^{+/0}$ and one reversible reduction event at ≈−1.7 V vs $Fc^{+/0}$ are observed for azo-OMe. In the presence of 1 eq TFA, an irreversible reduction event is observed at −0.8 V vs $Fc^{+/0}$, a 900 mV positive shift. Figures S6 and S7 show the current response during acid titration from 0 to 1.14 eq TFA in which the initial CV peak (at ≈−1.2 and −1.8 V vs $Fc^{+/0}$ for azo-OH and at ≈−1.7 V vs $Fc^{+/0}$ for azo-OMe) smoothly transitions to the final potential. Over the same range of TFA concentrations, anthracene shows no variation in the CV scans except for onset of proton reduction with increasing TFA (Figure S8). The large positive shift of the reduction event for azo-OH and azo-OMe is consistent with previous PCET studies of azobenzene.[20]

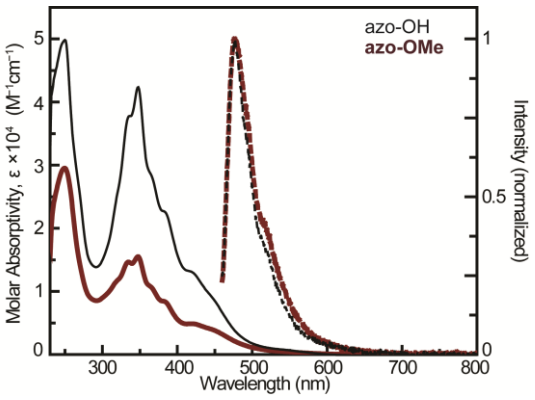

Figure 1. Molar Absorptivity (*solid*) and normalized emission (*dashed*) of azo-OH (*black*) and azo-OMe (*red, bold*).

Table 1. Summary of emission quantum yield and transient absorption data

	Emission QY%	τ_1(Error*) /ps	τ_2(Error*) /ns
azo-OH	0.55 (0.10)	3.5 (0.6)	2.5 (0.5)
azo-OH/TFA	0.79 (0.10)	3.0 (0.5)	2.9 (2.2)
azo-OMe	0.33 (0.04)	3.7 (0.2)	2.5 (0.8)
azo-OMe/TFA	0.37 (0.03)	3.8 (0.3)	2.6 (1.8)

*Error reported with 95% confidence intervals of at least three measurements.

Spectroelectrochemical (SEC) data was acquired of azo-OH, azo-OMe, and anthracene in acetonitrile with a 0.1 M $TBAPF_6$ with 0 and 1 eq TFA and are shown in Figure S9, S10 and S11. In azo-OH oxidative spectra, a bleach of the neutral species appears at ≈350 nm as does the growth of a peak associated with the oxidized species at ≈500 nm. The azo-OH radical cation at ≈500 nm is also observed in the presence of TFA. The reductive SEC spectra of azo-OH also show the bleach seen at ≈350 nm and the growth of a peak associated with the reduced species at ≈500 nm. The oxidative SEC spectra of azo-OMe shows a bleach of the neutral species at ≈325 nm and a growth of two peaks associated with the oxidized species at ≈375 nm and ≈475 nm in the absence and presence of TFA. The reductive SEC spectra showed a bleach of the neutral species and a growth of two peaks corresponding to the reduced species at ≈475 nm and ≈600 nm in the absence and presence of TFA.

Transient absorption (TA) spectroscopy was performed on azo-OH and azo-OMe in acetonitrile under a nitrogen environment with 0 and 5 eq of TFA. Figure 3 shows the TA evolution over the first 5 ns after excitation for azo-OMe with 0 eq TFA. The corresponding spectra for azo-OH (0 eq and 5 eq TFA) and azo-OMe (5 eq TFA) are similar and are shown in Figure S12. TA spectra of azo-OH with 0 and 5 eq TFA reveal a relatively narrow induced absorption at ~475 nm and a broader peak centred at 600 nm. Both peaks decay concomitantly to the baseline within the 5-ns temporal window. The expected ground-state bleach at ~450 nm is obscured by the induced absorption. The azo-OMe TA spectra share similar features to those of the azo-OH, both in the absence and presence of TFA. Again, peaks at ~475 nm and ~600 nm decayed concurrently to the baseline. The ground state bleach of azo-OMe is obscured by the induced absorption.

Global analysis was performed on the TA data to produce decay-associated difference spectra (DADS) with associated lifetimes for azo-OH and azo-OMe with both 0 and 5 eq TFA. The DADS and their lifetimes are shown in Figure S12. Table 1 summarizes the average global analysis lifetimes. Global analysis fitting produces two components, with lifetimes of ~3.0-3.8 ps and 2.5-2.9 ns. The shorter ~3 ps lifetime is the heavily dominant component. This DADS shows peaks that are coincident with the induced absorptions of the TA spectra (~475 nm and a broader peak centred at 600 nm). The 2.5 ns component accounts for less than 10% of the signal and resembles the very small residual spectrum that is barely visible

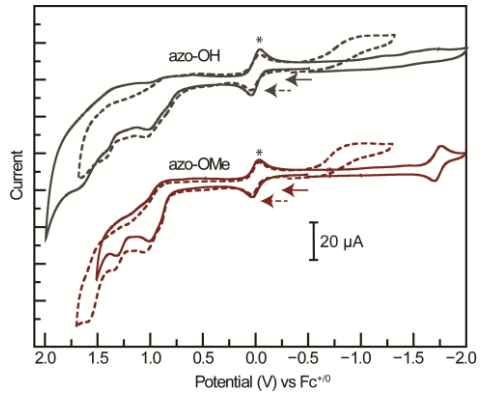

Figure 2. Cyclic voltammetry of 0.5 mM azo-OH (*top, solid*) and 0.5 mM azo-OMe (*bottom, solid*) in 100 mM $TBAPF_6$ in ACN at 100 mV/s under N_2 and with 1 eq TFA (*dashed*). The star notes the $Fc^{+/0}$ couple.

in the TA spectra themselves.

The excited-state dynamics do not change significantly between the 0 and 1 eq TFA azo-OH and azo-OMe samples. The shorter, dominant excited state component (~3.0-3.5 ps) represents the excited state of these azo dye dyads. This excited state may be due to a charge-transfer state produced directly upon excitation or a photo-induced ET/PCET, however, this assignment cannot be made with confidence using the data available at this time. While the azo-OMe DADS resemble the reductive SEC spectrum (vide supra), the DADS of azo-OH do not resemble the oxidative or reductive SEC spectra. Furthermore, the immediate formation of the observed excited state with rapid decay is not consistent with a photo-induced ET process that would instead produce a growth and subsequent decay of an intermediate charge-transfer state. The lack of a photo-induced charge transfer state could be attributed to a highly delocalized ground and excited states verified by computational methods (vide infra). Further, a rapid trans/cis isomerization may outcompete the charge transfer process leading to the rapid excited-state deactivation. Further experiments are currently underway to elucidate the nature of the excited state.

Density functional theory (DFT) and time-dependent DFT (TDDFT) calculations were performed using the B3LYP functional[24–26] and 6-311G(d,p) basis set[27–30] utilizing a PCM solvation model to simulate an acetonitrile solvent environment. Molecular orbitals of HOMO−2 through LUMO+2 (Figure S13-S14) of azo-OH and azo-OMe show electron density is delocalized across the entire molecule, except for the HOMO-2 orbital of the unprotonated dye, in which orbital density is localized on the azo linkage and LUMO+1, which shows minimal density on the phenyl group (Figure 4). To gain insight to the electronic structure of the protonated azo dyes, DFT and TDDFT calculations were performed on the dyes, in which the nitrogen adjacent to either the phenol/4-methoxyphenyl or the anthracene was modelled as protonated. In all protonated azo dye dyads, the HOMO−2 is no longer localized on the azo bond, but is instead completely delocalized. In similar fashion to the unprotonated azo dyes, the protonated species show delocalized orbital density in the HOMO to HOMO−1 occupied orbitals. TDDFT calculations show that the primary absorption features of the unprotonated species (300 nm-500 nm) result from transitions between states of highly delocalized electron density. These transitions occur primarily between frontier and HOMO−1/LUMO+1 orbitals, with the HOMO-LUMO transition at 458 nm. The predicted transitions strongly resembles the experimental spectrum (Figure 4). The calculated, lowest energy transition of the protonated species shows a dramatic red shift compared to the unprotonated state. In both dyes, protonated at either position, the absorbance spectrum is predicted to redshift. The HOMO-LUMO transitions of the protonated species is predicted to shift below 600nm (Figure S17).

The photochemical and electrochemical behaviour of these anthracene-based azo dye dyads diverge in the foregoing analysis. While electrochemistry reveals a dramatic shift in the reduction potential with the addition of 1 eq TFA, the photochemistry shows essentially no change. That reducing the dyads is easier with the addition of the positively charged proton follows from PCET precedent and may indicate a concerted PCET electrochemical process. Indeed, DFT corroborates this experimental observation, producing more stabilized LUMO levels in the protonated dyads. However, the observed photochemistry stands in contrast. Although DFT energy levels show an overall reduction of the HOMO-LUMO gap upon protonation, the measured absorption spectra of the azo dyes do not shift with addition of 1 eq TFA. Further, TA spectroscopy shows virtually no difference in excited-state spectra or lifetimes of the sample containing 1 eq TFA. While the cause for these disparate observations is still unclear, it is likely that the neutral azo-dyes are not protonated with addition of only 1 eq TFA.

An essential consideration in photo-induced ET or PCET is the driving force. That is, the excited state of the dyad must deliver sufficient driving force to induce ET between the donor (phenol/4-methoxyphenyl) and acceptor (anthracene). The excited-state energy of azo-OH and azo-OMe is ~2.76 eV, approximating the excited-state energy using the overlap of the normalized absorption and emission spectra (~450 nm). This excited-state energy is lower that what might be expected for anthracene-based systems owing to the red-shifted band in these highly conjugated dyads. The driving force for ET, based on the difference between the reduction and oxidation potentials of the constituent moieties, is 2.2 eV and 2.7 eV for

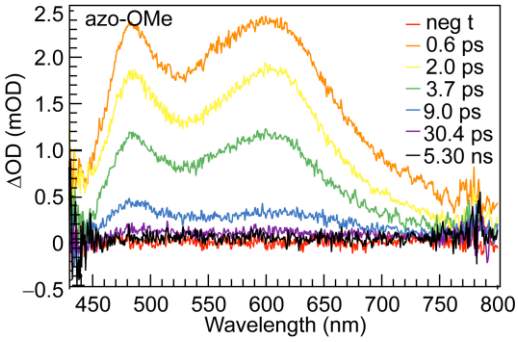

Figure 3. Transient absorption spectra for azo-OMe (azo-OH closely resembles the azo-OMe data and is shown in Figure S12). Samples were 30 µM in azo dye and prepared under a nitrogen environment in a 2-mm quartz high-vacuum cuvette. Samples were excited at 370 nm.

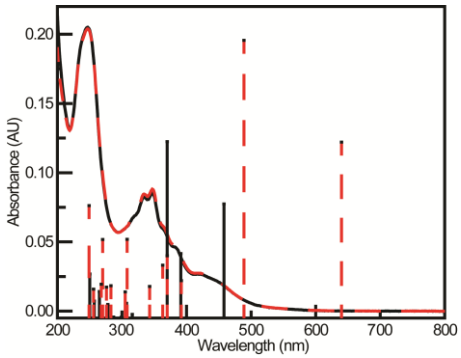

Figure 4. Absorption spectra of azo-OMe in the absence (*black*) and presence (*red, dashed*) of 1 eq of TFA, overlaid with predicted transitions from TDDFT from unprotonated (black) and protonated (red, dotted) dyes.

azo-OH and azo-OMe, respectively. The azo-dye dyads with 0 eq TFA possess between 0.5 and 0.05 eV driving force. However, upon addition of TFA, the reduction potential is increased and the PCET driving force to is reduced to 1.8 eV for both azo dyads. The ability to dramatically tune the driving force for photo-induced PCET is a compelling feature of this azo dye-based system.

Our experimental observations merit a modified design for achieving photo-induced PCET using azo-linkages. Modified model systems should electronically decouple the donor and acceptor moieties to break the highly conjugated ground and excited states and prevent possible trans/cis isomerization. Strategies to achieve this goal are currently under consideration for future efforts.

In conclusion, we report the design, synthesis and characterization of anthracene-based azo dye dyads, azo-OH and azo-OMe, for the mechanistic study photo-induced PCET. Electrochemical measurements show that the azo-OH and azo-OMe reduction potentials shift dramatically upon addition of acid. However, the photochemistry of the dyads shows little dependence on the presence of 1 eq TFA. The anthracene and phenol/4-methoxyphenyl moieties of the azo dyes are highly conjugated, which minimizes the ability of the dyads to undergo photo-induced charge transfer, despite sufficient driving force. We suggest that design modifications could achieve an azo-based model system for photo-induced PCET.

Conflicts of interest

There are no conflicts to declare.

Acknowledgements

The authors thank the NSF Major Research Instrumentation program (CHE-1428633). We thank Prof. Lisa Fredin for helpful discussions about TDDFT and Prof. Jeanne Berk for molecular design inspiration.

References

1 N. S. Lewis and D. G. Nocera, *Proc. Natl. Acad. Sci.*, 2006, **103**, 15729–15735.

2 S. Y. Reece, J. M. Hodgkiss, J. Stubbe and D. G. Nocera, *Philos. Trans. R. Soc. B*, 2006, **361**, 1351–1364.

3 S. Ye, R. Chen, Y. Xu, F. Fan, P. Du, F. Zhang, X. Zong, T. Chen, Y. Qi, P. Chen, Z. Chen and C. Li, *J. Catal.*, 2016, **338**, 168–173.

4 S. Ye, C. Ding, R. Chen, F. Fan, P. Fu, H. Yin, X. Wang, Z. Wang, P. Du and C. Li, *J. Am. Chem. Soc.*, 2018, **140**, 3250–3256.

5 A. Pannwitz and O. S. Wenger, *J. Am. Chem. Soc.*, 2017, **139**, 13308–13311.

6 J. M. Mayer, *Annu. Rev. Phys. Chem.*, 2004, **55**, 363–390.

7 J. J. Warren and J. M. Mayer, *Biochemistry*, 2015, **54**, 1863–1878.

8 O. S. Wenger, *Accounts Chem. Res. Res.*, 2013, **46**, 1517–1526.

9 J. C. Lennox, D. A. Kurtz, T. Huang and J. L. Dempsey, *ACS Energy Lett.*, 2017, **2**, 1246–1256.

10 J. L. Dempsey, J. R. Winkler and H. B. Gray, *Chem. Rev.*, 2010, **110**, 7024–7039.

11 R. Gera, A. Das, A. Jha and J. Dasgupta, *J. Am. Chem. Soc.*, 2014, **136**, 15909–15912.

12 T. T. Eisenhart and J. L. Dempsey, *J. Am. Chem. Soc.*, 2014, **136**, 12221–12224.

13 S. Luber, K. Adamczyk, E. T. J. Nibbering and V. S. Batista, *J. Phys. Chem. A*, 2013, **117**, 5269–5279.

14 S. K. Yesodha, C. K. Sadashiva Pillai and N. Tsutsumi, *Prog. Polym. Sci.*, 2004, 29, 45–74.

15 H. Mustroph, M. Stollenwerk and V. Bressau, *Angew. Chemie Int. Ed.*, 2006, **45**, 2016–2035.

16 Y. Ali, S. A. Hamid and U. Rashid, *Mini-Reviews Med. Chem.*, 2018, **18**, 1548–1558.

17 V. M. Dembitsky, T. A. Gloriozova and V. V Poroikov, *Nat. Products Bioprospect.*, 2017, **7**, 151–169.

18 L. Zhang and J. M. Cole, *ACS Appl. Mater. Interfaces*, 2014, **6**, 3742–3749.

19 J. L. Sadler and A. J. Bard, *J. Am. Chem. Soc.*, 1968, **90**, 1979–1989.

20 J.-M. Savéant and C. Tard, *J. Am. Chem. Soc.*, 2014, **136**, 8907–8910.

21 S. Concilio, L. Sessa, A. M. Petrone, A. Porta, R. Diana, P. Iannelli and S. Piotto, *Molecules*, 2017, **22**, 875–887.

22 D. Abdallah, J. Whelan, J. M. Dust, S. Hoz and E. Buncel, *J. Phys. Chem. A*, 2009, **113**, 6640–6647.

23 B. D. McCarthy and J. L. Dempsey, *Inorg. Chem.*, 2017, **56**, 1225–1231.

24 C. Lee, C. Hill and N. Carolina, *Chem. Phys. Lett.*, 1989, **162**, 165–169.

25 L. S. Kassel, *J. Chem. Phys.*, 1936, **4**, 276–282.

26 F. J. Devlin, J. W. Finley, P. J. Stephens and M. J. Frisch, *J. Phys. Chem.*, 1995, **99**, 16883–16902.

27 R. Ditchfield, W. J. Hehre and J. A. Pople, *J. Chem. Phys.*, 2004, **54**, 724–728.

28 M. M. Francl, W. J. Pietro, W. J. Hehre, J. S. Binkley, M. S. Gordon, D. J. DeFrees and J. A. Pople, *J. Chem. Phys.*, 1982, **77**, 3654–3665.

29 W. J. Hehre, K. Ditchfield and J. A. Pople, *J. Chem. Phys.*, 1972, **56**, 2257–2261.

30 P. C. Hariharan and J. A. Pople, *Theor. Chim. Acta*, 1973, **28**, 213–222.